J. Neural Eng. **10** (2013) 045002 (16pp) doi:10.1088/1741-2560/10/4/045002

3D Parylene sheath neural probe for chronic recordings

B J Kim[1], J T W Kuo[1], S A Hara[1], C D Lee[1], L Yu[1], C A Gutierrez[2], T Q Hoang[1], V Pikov[3] and E Meng[1,4,5]

[1] Department of Biomedical Engineering, University of Southern California, 1042 Downey Way, DRB-140, Los Angeles, CA 90089-1111, USA
[2] Independent Consultant, Los Angeles, CA 90017, USA
[3] Huntington Medical Research Institutes, 734 Fairmount Avenue, Pasadena, CA 91105-3104, USA
[4] Ming Hsieh Department of Electrical Engineering, University of Southern California, 3740 McClintock Ave, EEB-100, Los Angeles, CA 90089-2560, USA

E-mail: ellis.meng@usc.edu

Received 29 January 2013
Accepted for publication 10 April 2013
Published 31 May 2013
Online at stacks.iop.org/JNE/10/045002

Abstract

Objective. Reliable chronic recordings from implanted neural probes remain a significant challenge; current silicon-based and microwire technologies experience a wide range of biotic and abiotic failure modes contributing to loss of signal quality. *Approach.* A multi-prong alternative strategy with potential to overcome these hurdles is introduced that combines a novel three dimensional (3D), polymer-based probe structure with coatings. Specifically, the Parylene C sheath-based neural probe is coated with neurotrophic and anti-inflammatory factors loaded onto a Matrigel carrier to encourage the ingrowth of neuronal processes for improved recording quality, reduce the immune response, and promote improved probe integration into brain tissue for reliable, long-term implementation compared to its rigid counterparts. *Main results.* The 3D sheath structure of the probe was formed by thermal molding of a surface micromachined Parylene C microchannel, with electrode sites lining the interior and exterior regions of the lumen. Electrochemical characterization of the probes via cyclic voltammetry and electrochemical impedance spectroscopy was performed and indicated suitable electrode properties for neural recordings (1 kHz electrical impedance of ~200 kΩ *in vitro*). A novel introducer tool for the insertion of the compliant polymer probe into neural tissue was developed and validated both *in vitro* using agarose gel and *in vivo* in the rat cerebral cortex. *In vivo* electrical functionality of the Parylene C-based 3D probes and their suitability for recording the neuronal activity over a 28-day period was demonstrated by maintaining the 1 kHz electrical impedance within a functional range (<400 kΩ) and achieving a reasonably high signal-to-noise ratio for detection of resolvable multi-unit neuronal activity on most recording sites in the probe. Immunohistochemical analysis of the implant site indicated strong correlations between the quality of recorded activity and the neuronal/astrocytic density around the probe. *Significance.* The provided electrophysiological and immunohistochemical data provide strong support to the viability of the developed probe technology. Furthermore, the obtained data provide insights into further optimization of the probe design, including tip geometry, use of neurotrophic and anti-inflammatory drugs in the Matrigel coating, and placement of the recording sites.

(Some figures may appear in colour only in the online journal)

[5] Author to whom any correspondence should be addressed.

1. Introduction

Chronically implanted intracortical recording electrode arrays can facilitate basic neuroscience studies and also be used to bridge the gap between man and machine in the development of clinical brain–machine interfaces [1, 2]. These implanted neural probes are utilized to record extracellular electrical activity associated with limb-movement intent and to facilitate motor control for chronic neural prosthetic applications. However, to realize the potential of neural prosthetics, the technological challenge is to develop recording probes that maintain long-term functionality *in vivo*. The introduction of batch micromachining techniques to neural probe manufacturing has provided the crucial capability to fabricate precise probe shapes and electrode sizes that has improved long-term probe fidelity considerably [3–5].

Two silicon-based chronic probe technologies have enjoyed widespread adoption: the monolithic, 'bed-of-needles' Utah Electrode Array (UEA) [6] and the planar, multi-site Michigan Array (MA) [7]. The UEA consists of tapered-tip silicon needles insulated in a polymer, with exposed platinum electrodes at the tip and has found success in cats [8], non-human primates [9], as well as human subjects [10]. The MA also is formed using microfabrication techniques, but entails a sharp silicon shank with multiple electrode sites along the length of the shank designed with integrated CMOS electronics [11] and the capability of expanding to three dimensional (3D) array conformations [12]. These array platforms allow for a dense packing of recording sites and have demonstrated neural recordings in their respective models over years. However, reliable implementation of these devices has proven to be difficult as these chronically implanted neural probes are susceptible to a number of failure modes, reducing their longevity *in vivo*.

In addition to the device-based ('abiotic') failure modes (e.g. insulation delamination, electrode corrosion), several biological ('biotic') failure modes can further reduce the neural recording ability [13]. While the dominant mechanism for the gradual decay in the recording quality is still debated, most researchers agree that the immune response to the chronic presence of a foreign object in the brain plays an important role in this process [14, 15]. There is a considerable mechanical mismatch between the stiffness of the silicon or metal probe and soft cortical tissue, inflicting continuous damage to the brain microvasculature, extracellular matrix, and neurons [16, 17]. These inflammatory processes also contribute to the formation of a glial cell encapsulation, or 'glial scar', around the probe and the retraction of neurons from the probe, which prevents high fidelity recordings [18]. Tethering between skull anchoring of electrical connectors and the implanted probe further contributes to adverse micromotion or development of interfacial stresses between the stiff neural probes and cortical tissue [19].

Efforts to mediate these failure modes directed the development of softer probe materials and novel designs for chronic neural probes. Polymer-based neural probes [20–24] constructed on compliant substrates (e.g. polyimide, Parylene C, liquid crystal polymer) and novel probe architectures [25–27] were pursued to further improve tissue integration *in vivo*. Interestingly, a glass-based probe technology, the neurotrophic cone electrode (NE), was successfully demonstrated in chronic applications in both animals and humans and is attributed to the unique hollow conical tip coated with growth factors [28–33]. The NE consists of a glass cone with microwire electrodes manually placed within the inner lumen of the cone. The cone is coated with neural growth factors to promote the growth of neural processes toward the electrodes as well as to allow for better integration with the cortical tissue. The release of these factors by the neural probe *in vivo* may counteract the adverse physiological responses reported in other chronically implanted probes. By having the ingrowth of neurons closer to the electrode sites over time, improved neural signal quality can be achieved as the distance between the neurons and electrodes is decreased [34]. Also, the effects of micromotion are diminished as the growth of tissue within and through the cone facilitate integration and anchoring of the probe with the surrounding tissue.

The NE however, requires a manual and labor intensive process for its fabrication and possesses a rigid glass structure with a large mechanical mismatch with surrounding neural tissue. By taking advantage of micromachining processes and polymer construction, we previously demonstrated the feasibility of constructing a NE-like probe shape based on the flexible substrate, Parylene C (hereto referenced as Parylene) [35]. It is the aim of the 3D Parylene-based sheath probes to employ the sheath design and neural ingrowth concept of the NE but with a polymer-based substrate to improve tissue integration and allow more reliable, long-term performance *in vivo*. Here, a new design of the Parylene sheath probes with improved mechanical robustness and their *in vivo* implementation for neural recording are described. The 3D Parylene sheath probe consists of a hollow sheath structure with electrode sites decorating the inner lumen as well as the outer perimeter of the sheath. By utilizing the thermoplastic nature of Parylene [36], an as-fabricated, flat Parylene microchannel was thermally formed via a post-processing step into a 3D sheath structure. Because of Parylene's compatibility with microfabrication techniques, probes with precise designs can be batch fabricated to ensure probe-to-probe repeatability and thus increased reliability. An extended Parylene ribbon cable from the sheath probe tip allowed additional flexibility and terminated in a linear contact pad array for establishing electrical connections to the neural probe (figure 1). Sheaths were similarly coated with neurotrophic factors and anti-inflammatory agents with the aim to encourage neural ingrowth into the sheath and/or inhibit inflammation, respectively.

2. Materials and methods

2.1. Fabrication of parylene sheath probe

The 3D Parylene sheath neural probe with integrated Parylene cable was surface micromachined using a two-dimensional layer-by-layer process, building upon a supported Parylene

substrate to form a Parylene sheath (figure 2). Parylene was chosen as the probe substrate and structural material because of its USP class VI rating, compatibility with micromachining processes [37], and flexibility to improve the mechanical mismatch between the probe and tissues [38]. Following a dehydration bake (120 °C, 20 min) a 5 μm layer of Parylene (Specialty Coating Systems, Indianapolis, IN) was deposited on a bare silicon wafer with its native oxide layer intact. The native oxide aided release of these sheath probes off of the wafer. Platinum (Pt) metal (2000 Å) was deposited using e-beam evaporation and patterned using photolithography and a lift-off process to pattern the inner and outer electrodes (45 μm diameter), leads (10 μm width), and contact pads (350 μm × 3.5 mm). Platinum was chosen as the electrode material for its biocompatibility, inertness within biological environments [39], and long track record for neural recordings. A titanium adhesion layer was not used as Pt has been reported to have good adhesion with Parylene substrates [40], however O_2 plasma was used to treat and descum the surface prior to metal deposition [41]. Previously, the outer electrodes of the sheath probe were fabricated using a dual-layer liftoff technique on top of the sheath that allowed for continuous electrical wiring across the sidewall of the Parylene microchannel [35]. However, it was observed that the mechanical opening of the sheath during the fabrication post-processing produced tensile stresses sufficient to crack electrode sites for the probe dimensions investigated here. Therefore, outer electrodes were moved to the sheath perimeter. This design simplified the fabrication process, reduced probe fabrication time, and increased yield.

An insulation layer of Parylene (1 μm) was then deposited, patterned, and etched using O_2 plasma to expose the electrode sites as well as the contact pads. A thick sacrificial photoresist layer (∼10 μm) was spun on and patterned to form the microchannel structure that would later become the inner lumen of the 3D Parylene sheath. To form the top surface of the microchannel, a 5 μm layer of Parylene was deposited and openings were etched at both ends to form the final 2D sheath structure; in the same step the outer electrodes and contact pads were etched and exposed. The devices were then cut-out using O_2 plasma etching, defining the probe shape and cable length. The sacrificial photoresist was removed using a sequential soak in acetone, isopropyl alcohol, and deionized (DI) water to reveal the inner lumen of the sheath structure. Sheath probes were released from the wafer by gently peeling the Parylene devices from the carrier wafer while immersed in DI water.

Three designs with varying sheath shapes were evaluated (figure 3). Design A ('sharp taper'; 300 to 50 μm) and design B ('moderate taper'; 450 to 50 μm) are both conical in shape, with design B having a wider taper to explore the effects of a larger opening on one end of the sheath for neuronal growth as well as the impact of sheaths of different sizes. Design C is cylindrically-shaped ('blunt'), with openings of equal dimension (300 μm) at both ends of the sheath. It is expected that sharper tapers and smaller sizes will reduce damage and achieve better performance for chronic applications.

To form the 3D sheath shape from a 2D microchannel, the as-fabricated Parylene probe was thermoformed. By inserting a mold into the sheath and heating the sample above the glass transition temperature of Parylene (∼90 °C [42, 43]), the polymer chains are free to migrate and allow the film to conform to the shape of the mold. Following a slow cool down of the sample, the modified shape of the Parylene film was retained, even after the mold was removed—this resulted in a newly, thermoformed structure with an increased crystallinity (and thus stiffness) [44]. As Parylene undergoes thermal oxidative degradation in an oxygen environment at temperatures >125 °C [45], this process was performed in a vacuum oven with nitrogen backflow (10 SCFH).

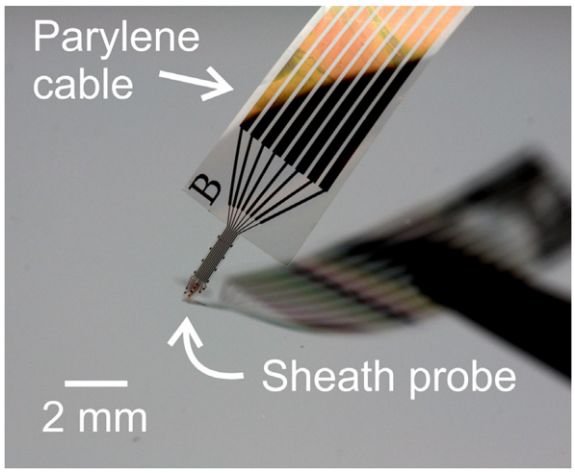

Figure 1. Photograph of 3D Parylene sheath probe highlighting the probe tip and a portion of the integrated Parylene cable.

Custom microwires were fabricated from tungsten (MicroProbes for Life Science, Gaithersburg, MD) and stainless steel (Cooner Wire Co., Chatsworth, CA) with tip ends shaped to match the specific taper designs (A, B, or C) and were used to thermoform the 3D sheath structures (figure 4). Following insertion of the microwire molds into the microchannel, the opened probes were placed within a vacuum oven (V0914A; Lindberg/Blue, Asheville, NC) and heated to 200 °C; the thermoforming step also serves to anneal Parylene layers [46] for improved adhesion and strength *in vivo*. Following thermal treatment and cooling, the molds were easily removed without the need for release agents (figure 4(c)), and probes were packaged for implantation.

2.2. *Packaging techniques*

Because of the soft Parylene substrate, traditional means of establishing electrical connections to contact pads that require heat and mechanical abrasion cannot be used. We previously presented a zero insertion force (ZIF) connection scheme that allowed for rapid, robust, and repeatable connections to multi-channel Parylene cables [47]. Utilizing this connection strategy, dual probe arrays were devised by using a flexible printed circuit board (flexPCB) with two ZIF connectors (FH19SC-8S-0.5SH(05); HIROSE Electric USA, Inc., Simi Valley, CA), one on each side of the flexPCB (figure 5). The contact pad region of the Parylene cable was first stiffened by affixing a polyetheretherketone sheet (8504K13; McMaster-Carr, Aurora, OH) to match the required cable thickness for the

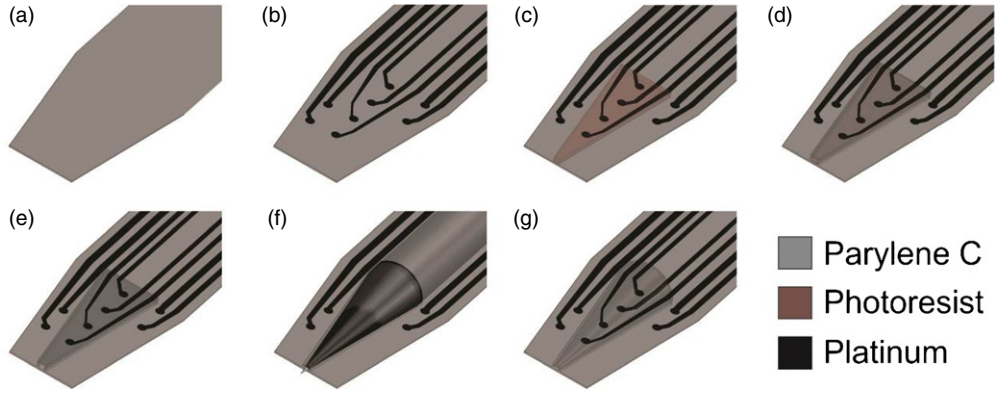

Figure 2. Overview of fabrication steps for 3D Parylene sheath probe. (Note: fabrication steps as drawn are shown on an already cut-out substrate, however the devices are not cut to shape during the actual process until step (d).) (a) 5 μm of Parylene was first deposited onto a carrier wafer. (b) Pt electrodes (2000 Å) were e-beam evaporated and patterned using lift-off. Parylene insulation (1 μm) was deposited and patterned to expose the electrode sites using O_2 plasma. (c) A sacrificial layer of photoresist was spun on and patterned to form the microchannel structure. (d) Parylene (5 μm) was deposited on top of the sacrificial layer to complete the microchannel. Openings were etched into the ends of the microchannel and the border of the device was also etched to form the final sheath structure and shape. (e) The sacrificial photoresist is removed using a sequential acetone, isopropyl alcohol, and DI water soak. The probes were then dried. (f) A microwire matching the taper width was inserted into the sheath to mechanically open and form the 3D sheath structure. (g) Following thermoforming, the microwire was removed.

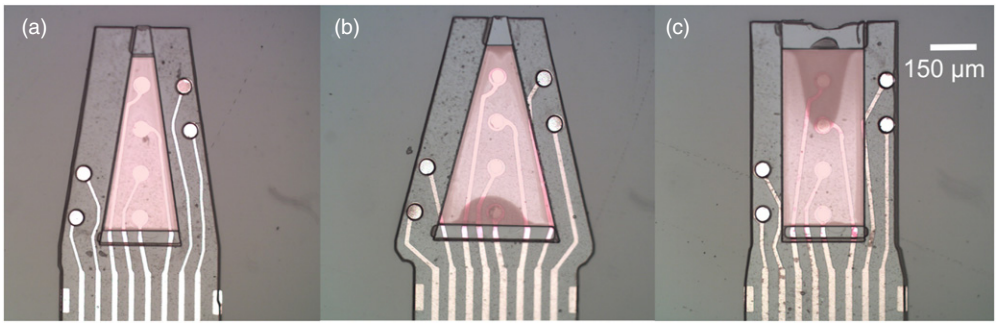

Figure 3. Photographs of the three probe designs investigated; probes are shown as-fabricated with photoresist sacrificial layer still intact: (a) 300 to 50 μm taper (A; 'sharp'), (b) 450 to 50 μm taper (B; 'moderate'), and (c) 300 μm cylinder (C; 'blunt').

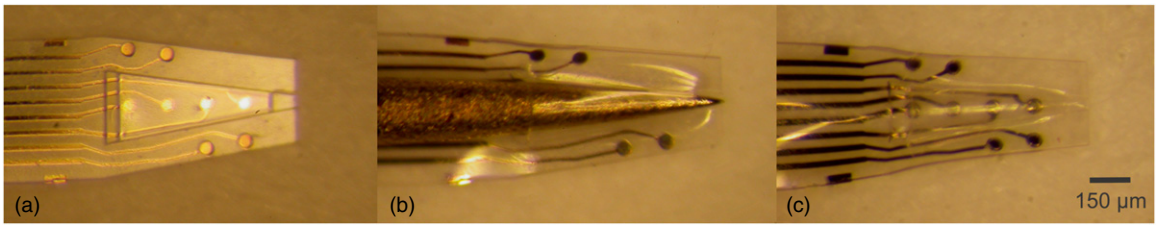

Figure 4. (a) Parylene sheath probe after release from wafer with flat 2D microchannel structure. (b) Microwire mold inserted into the microchannel for thermoforming process. (c) Thermoformed result showing opened 3D sheath structure.

ZIF connector. The stiffened cable was then inserted into the ZIF connector and locked into place by closing the actuator. A probe separation of 1 mm was set by the ZIF connector spacing on the flexPCB to match the rostro-caudal extent of the M1 motor cortex in the rat. This custom flexPCB was designed to allow the 16 channels of the dual probe array to interface to a contact pad layout for a 33 channel ZIF connector (FH26–33S-0.3SHW(05); HIROSE Electric U.S.A., Inc., Simi Valley, CA). An external ZIF-Omnetics adaptor PCB was used to connect the implanted dual probe array (ZIF) to the recording system (OmniPlex; Plexon Inc., Dallas, TX).

2.3. In vitro electrochemical characterization

The 3D Parylene sheath neural probes were characterized electrochemically using cyclic voltammetry (CV) and electrochemical impedance spectroscopy (EIS). The dual-probe arrays were connected to a potentiostat (Reference 600; Gamry Instruments, Warminster, PA) via a ZIF connector. CV was used to characterize the metal surface of the electrodes and also to clean electrode surfaces following the fabrication and post-processing steps [48]. CV was performed (voltage range −0.2 to 1.2 V, 250 mV s^{-1} scan rate, 30 cycles) for all electrodes of the dual array in a beaker of 0.05 M sulfuric

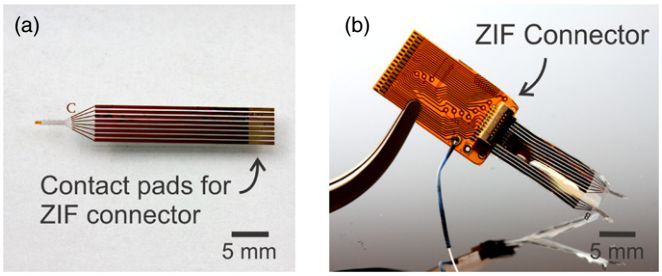

Figure 5. (a) As-fabricated Parylene sheath probe highlighting the contact pads for integration with ZIF connectors. (b) Photograph of fully packaged dual-probe array with two probes secured into two ZIF connectors on the flexPCB. Note the separation of the two probes was created by the spacing of the ZIF connectors on either side of the flexPCB. The flexPCB terminated in a contact pad layout designed for a 33 channel ZIF connector.

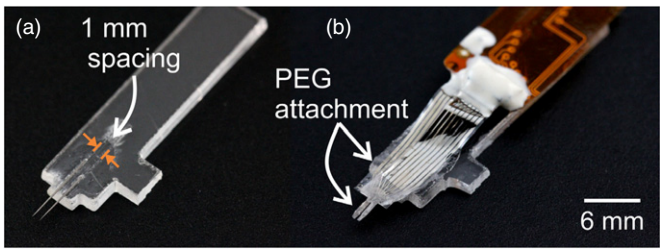

Figure 6. (a) A custom microwire-based introducer tool used for implantation for dual-probe array. (b) The dual-probe array was temporarily affixed to the introducer tool using PEG, which dissolved following insertion. PEG was used in two locations: cable region for strain relief and support and probe-microwire tip for stiffness during insertion.

acid (EMD Chemicals, Darmstadt, Germany) solution using a large-area (1 cm^2) Pt plate as the counter electrode and an Ag/AgCl electrode (RE-5B Ag/AgCl Reference Electrode; BASi, West Lafayette, IN) as the reference electrode. Electrode impedance serves as a good metric in determining electrode performance *in vivo* [13]. EIS was performed in a beaker of 1 × phosphate buffered saline solution (PBS; OmniPur 10 × PBS, EMD Chemicals, Darmstadt, Germany) with a 10 mV_{rms} excitation voltage over 1 Hz to 100 kHz. Again, a Pt plate served as the counter electrode and an Ag/AgCl electrode as the reference electrode.

2.4. Coating methods

For initial *in vivo* studies, three different coating mixtures were investigated to determine their effects on sheath probe efficacy, namely the enhanced integration of the probe *in vivo* by neural ingrowth. Coating variations consisted of a Matrigel (MG) (79% dilution in 1 × PBS; BD Bioscience, San Jose, CA) matrix containing either: (a) a neurotrophic cocktail (NTC) (rat nerve growth factor (NGF; 1 μg ml^{-1}; Sigma-Aldrich, St. Louis, MO) + neurotrophin-3 (NT-3; 1 μg ml^{-1}; Sigma-Aldrich, St. Louis, MO)); (b) water soluble dexamethasone (DEX) (2 mg ml^{-1}; Sigma-Aldrich, St. Louis, MO); or (c) no additives. Non-coated probes were used as a control. MG, an extracellular matrix, was used because of its inherent ability to support the growth of cells [49] and for convenience in adding factors. Two neuronal growth factors (NGF and NT-3) in the NTC were chosen in an effort to encourage the growth of neuronal processes toward and into the sheath probe. Lastly, DEX was chosen to limit the immune response induced by the insertion and chronic presence of the probe.

To coat the sheaths, probe tips of the array were immersed in their corresponding coating solutions within a sonicator bath (1510 Branson; Emerson Industrial Automation, St. Louis, MO) at 4 °C, as MG is a gel at room temperature [49]. After sonicating in solution for 5 min to ensure an even coating, probe tips were removed from the solution and brought to room temperature for another 5 min to allow the coating to gel onto the sheath probe.

2.5. In vitro insertion tests

Although the Parylene substrate aids in the long-term integration of the probe *in vivo*, an issue arises in the insertion of a flexible structure into cortical tissue. Because of the compliance of the sheath probe, additional assistance is required to possess temporary stiffness during tissue penetration for a straight path into the desired depth into tissue to minimize tissue damage caused by buckling and movement during insertion [50]. Accordingly, an introducer tool was developed, made of a custom acrylic shuttle with laser-etched grooves for two tungsten microwires (250 μm diameter; MicroProbes for Life Science, Gaithersburg, MD) (figure 6(a)) designed for probe mounting. These microwires were also spaced 1 mm apart (set by the etched grooves) to allow for proper spacing of the probes during implantation to target the M1 motor cortex. The dual-probe array was temporarily attached to the introducer tool using polyethylene glycol (PEG) at two different points: (1) PEG 1000 (Carbowax^{TM} Sentry^{TM}; MW 1000, The DOW Chemical Company, Midland, MI) at the Parylene cable-acrylic interface for strain relief and robustness, and (2) an overcoat of PEG 8000 (PEG; MW 8000, Sigma-Aldrich, St. Louis, MO) mounted the probe to the side of the microwire to provide temporary stiffness during implantation (figure 6(b)). The overcoat at the probe-microwire interface also protects the coatings from shear-induced delamination during implantation. Attachment of the dual-probe array to the introducer tool was carried out under magnification to ensure that the depths were consistent from assembly to assembly. Following insertion of the probes, the PEG was dissolved using saline, allowing for removal of the introducer tool from the tissue.

In *in vitro* insertion experiments, 0.5% agarose (A9539–50G; Sigma-Aldrich, St. Louis, MO) gel brain phantom was used to mimic the mechanical consistency of the brain tissue [51, 52]. The PEG affixed dual-probe array was placed onto a stereotaxic frame and positioned over the agarose gel. The probe was lowered into the agarose by hand to a depth of 2 mm, and was followed by a saline flush to dissolve the PEG. After a short, 5 min wait period to ensure the complete dissolution of PEG, the introducer tool was withdrawn to leave the dual-probe array implanted within the agarose.

Table 1. Experimental groups. Numbers indicate how many animals were included in the analysis. Each animal was implanted with an array containing two probes with same tip shape and coating. In some animals, only one probe was functional.

Tip shape\Coating	MG only	MG + NTC	MG + DEX
A (Sharp)	4		
B (Moderate)	3	3	2
C (Blunt)	2		

2.6. Chronic cortical implantation

In vivo electrophysiological measurements were carried out to validate the efficacy and long term feasibility of the 3D Parylene sheath neural probes and to evaluate the three probe designs and three coating compositions. 19 young, male Sprague Dawley rats (>320 g) were implanted with dual-probe arrays, of which 13 animals were included in the analysis, with the other six excluded because of the flexPCB breakage ($n = 3$) and headplate becoming loose (due to a small number of screws used in earlier implants) ($n = 3$). All procedures for the animal experiments were in accordance with the animal protocol approved by the Huntington Medical Research Institutes Institutional Animal Care and Use Committee (HMRI IACUC) and in compliance with the Animal Welfare Act. The dual-probe arrays were subdivided into the following coating groups (table 1).

Comparison of the coatings was carried out using B-type probes, and comparison of the probe tip shapes was conducted using MG only-coated probes. Dual probe arrays were affixed to an introducer tool as described in the previous subsection. The array-tool assembly was ethylene-oxide sterilized for 24 h using a room-temperature sterilizing system (Anprolene AN74i, Andersen Products, Haw River, NC) and stored in sterile packaging at 4 °C until the time of implantation (∼1–2 days) following manufacturer specifications to reduce the degradation rate of the coatings [53]. The chronic implantation surgery was performed in the rat M1 motor cortex as follows. Anesthesia was induced by placing the rat in a chamber filled with 4% isoflurane in 1 lpm oxygen. The animal was then placed in a stereotaxic frame (Small animal stereotaxis; Kopf Instruments, Tujunga, CA) and 1–3% isoflurane in 1 lpm oxygen was administered via a nose cone. Following a 2 cm long midline incision and retraction of the skin, six holes were drilled into the skull to allow for attachment of a headplate (used as reference/ground) with six stainless steel screws. A craniotomy was made centered at +1.5 mm AP and 1.5 mm ML from bregma, exposing the M1 cortex. The dura layer over the target area was incised and retracted. The array-tool assembly was positioned over the opening region via a stereotaxic apparatus and manually inserted into the cortex with a micromanipulator until reaching the required depth of 2 mm under visual inspection using binocular loupes (Kepler 6.0x; Care-Optics Industrial Co., Ltd, Shenzhen, China). Following insertion, Kwik-Sil (World Precision Instruments, Sarasota, FL) was applied by syringe to the dual-probe array to anchor it in the cortex. After allowing 5 min for Kwik-Sil curing, saline was applied to allow for PEG dissolution and separation of the dual-probe array from the introducer tool. The tool was then withdrawn. Additional Kwik-Sil was applied to seal the craniotomy and for cable support. Bone cement was applied to anchor the array completely within a head cap. The skin was then closed around the implanted assembly and sutured shut (4-0 Nylon Monofilament sutures; Keebomed Inc., Morton Grove, IL). The animal was kept on a warming pad in a recovery cage until it was fully awake and sternal, at which point the animal was returned to its housing cage.

2.7. In vivo electrochemical and electrophysiological evaluation

To assess the functionality of the 3D Parylene sheath dual-probe array, *in vivo* EIS and neural recordings were carried out weekly, starting at day 0 in three animals and at day 7 in the remaining animals and ending at day 28 post-implantation. The collected data were used to calculate the performance metrics: impedance at 1 kHz, unresolved neural noise, signal-to-noise ratio (SNR), and event rate. These metrics were used to compare and down-select the probe shape, coating, and recording site placement. For the electrochemical/electrophysiological measurements, rats were anesthetized with Ketamine/Xylazine (90/10 mg/kg, IP). *In vivo* EIS measurements were obtained using a PC4/300 potentiostat system (Gamry Instruments, Warminster, PA) in a two-electrode configuration, with the reference and counter connected to the titanium headplate and its six transcranial stainless steel screws. The data were collected with 10 mV_{rms} sinusoids at the frequencies from 1 Hz to 100 kHz. The impedance values at 1 kHz were selected for analysis due to the physiological relevance of this frequency [14].

The electrophysiological data was acquired at 16 bit and 40 kHz per channel using a 64-channel data acquisition system (OmniPlex; Plexon Inc., Dallas, TX) and high-pass filtered at 300 Hz to remove the low-frequency fluctuations from the baseline. In the 120 s data records, spike detection was performed using the nonlinear energy operator (NEO) method, which allows more accurate spike detection at low SNRs as compared to a more commonly used amplitude thresholding method [54]. The spike detection threshold was set at 14 times the standard deviation of the NEO values in the record. The neuronal noise was calculated as the standard deviation of the data after removal of 0.8-msec-long segments containing the detected spikes. The spike amplitude was calculated as the absolute value of spike's peak height. The average spike amplitude for the record was calculated using all detected spikes. Spike sorting was not applied to remove false positives, as the data was collected while the rats, along with the connected headstage and pre-amplifier, were placed in a Faradaic cage, eliminating externally-generated electromagnetic interference at the Hz–kHz frequency range. Furthermore, there were no electromyographic artifacts, as the Ketamine/Xylazine anesthesia was sufficiently deep to suppress animal movements. Since both the average spike amplitude and average noise were calculated as monophasic values (as opposed to the biphasic peak-to-peak amplitude calculation), the SNR was calculated simply as the ratio of

these values. The event rate was also calculated for all spike-like events. The SNR and event rate values were calculated for a record only if ten or more spike-like events were detected in 120 s.

2.8. Immunohistochemical evaluation of the cortical implant sites

Within an hour after the last electrophysiological test, the rats were injected with heparin sulfate (1000 IU kg^{-1}, IP), while still anesthetized with Ketamine/Xylazine (90/10 mg/kg, IP), and transcardially perfused with 100 ml of a prewash containing phosphate buffered saline with heparin (5 IU ml^{-1}) followed by 200 ml of phosphate buffered 4% paraformaldehyde solution. The head was removed and immersion-fixed in 4% paraformaldehyde overnight. The next day, cerebral cortex dissection was performed. An effort was made to keep the probe inside the cortex during the removal of the bone cement-encapsulated flexPCB. In several cases, however, the probe came out from the cortex due to a lack of any connective tissue ingrowth holding it in place. The cortical tissue block containing the probe tracks (and occasionally the probes) was embedded into paraffin. The tissue was sectioned perpendicular to the probe tracks and the sections were microphotographed. The sections were then immunostained for GFAP (marker for reactive astrocytic processes) and visualized using Vector nickel-DAB, and for NeuN (neuronal marker) and visualized using Vector Red. The sections, single-stained with GFAP or NeuN, were subjected to semi-automated image analysis using software, custom-written in Visual Basic 6.0 (Microsoft Co., Redmond, WA) using National Instruments Image ActiveX component (National Instruments Co., Austin, TX). Within the software, a rounded rectangle was placed on the image for use during analysis; its placement, width and length were adjusted to match the perimeter of the probe track.

For NeuN quantification, a larger concentric rounded rectangle was automatically drawn at 300 μm distance from the inner one. The user manually clicked on all NeuN-stained neurons with clearly-visible nucleolus in the area between the rounded rectangles. The custom software then computed the distances of these neurons from the perimeter of the inner rounded rectangle and calculated the density of neurons in six 50-μm-wide areas around the inner rounded rectangle. The key NeuN measure was the ratio of neuronal density in the second inner-most area (spanning from 50 to 100 μm) to the average density in two outer-most areas (spanning from 200 to 300 μm).

For GFAP quantification, six larger concentric rounded rectangles were automatically drawn at 50 μm incremental distances from the inner one and the GFAP density was automatically calculated in these six areas. The key GFAP measure was the ratio of the average GFAP density in two inner-most areas (from 0 to 100 μm) to the average density in two outer-most areas (from 200 to 300 μm).

In addition to single-stained sections used in the image analysis, several sections in each tissue block were double-stained for publication purposes. Since the immunostaining process involves repeated rinses, in most cases the fragments of the Parylene probes were washed out from the tissue. Therefore, to illustrate a co-localization of the tissue and the probe, an image processing technique was used to merge the probe cross-sectional view from the unstained microphotograph with the surrounding tissue from the immunostained microphotograph.

2.9. Statistical analysis

The comparison between two groups (e.g. inner versus outer recording sites) was done using a two-tailed equal-variance *t*-test (built-in Excel function; Microsoft Co., Redmond, WA), while the comparisons among multiple groups (e.g. tip geometries and coating types) were done using Repeated Measures General Linear Model (SPSS; SPSS Inc., Chicago, IL), followed by Bonferroni post-hoc tests. Comparisons between the probe performance metrics (e.g. probe yield and SNR) and immunohistochemical metrics (e.g. relative neuronal and astrocyte density around the probe) were done using the square of Pearson's correlation coefficient, R^2, between the data and its best linear regression fit. The significance levels of 0.05, 0.01 and 0.001 were used. The normality of data was confirmed as an initial pre-requisite for performing the general linear model analysis.

3. Results

3.1. Fabrication

3D Parylene sheath neural probes were fabricated with eight circular electrodes (diameter = 45 μm), with four electrodes within the lumen of the Parylene sheath and four on the perimeter of the sheath. Dimensions were chosen such that following implantation the electrodes would be positioned in the layers IV–VI of the rat M1 cortex. Thermoforming with a microwire mold resulted in 3D sheath structures (figure 7), and also improved Parylene–Parylene adhesion (data not shown) to mitigate the delamination effects encountered by Parylene–Parylene interfaces within a wet environment [55]. The stiffness of the structure also increased sixty times corresponding to increased crystallinity resulting from thermal treatment of Parylene [56]. However, the sheath was still flexible enough to deflect to its original shape following deformation (figure 8) and did not contribute significantly to the overall stiffness of the probe.

3.2. Electrochemical characterization

The electrical packaging scheme utilizing the ZIF connection method and flexPCB was validated by successful electrochemical characterization. CV results indicated the characteristic curve for a Pt metal in a sulfuric acid solution, identified by its hydrogen adsorption and desorption peaks and its platinum oxidation and oxide reduction peaks (figure 9). The resulting CV cleaning of the electrode surface was demonstrated in the removal of multiple time constants and discontinuities in EIS magnitude and phase plots (figure 10), as the CV helps to reduce impedance

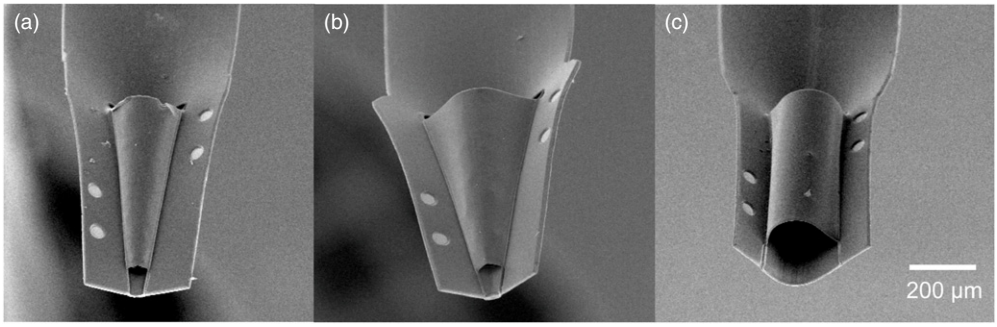

Figure 7. SEM images of the three different 3D thermoformed Parylene sheath probe designs: (a) A, (b) B, and (c) C that highlight the final 3D shape achieved following thermoforming.

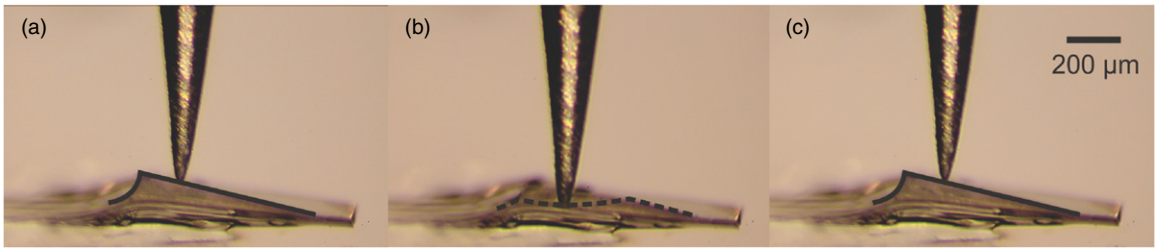

Figure 8. Sequential photographs (side-view of probe) demonstrating the mechanical robustness of the stiffened cone structure. (a) A deflection probe positioned above the sheath probe. (b) 100 μm displacement of the top of the sheath with the deflection probe. (c) Retraction of the deflection probe allowed the sheath to return to its original shape. Sheath movement is highlighted with a black outline.

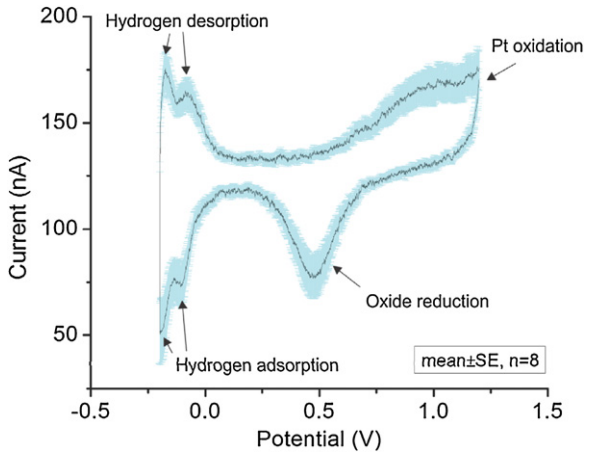

Figure 9. A cyclic voltammogram of a Pt electrode (mean ± SE, n = all 8 electrodes of single sheath probe) of the 3D Parylene sheath probe taken in a beaker of 0.05M sulfuric acid solution (voltage range = −0.2 to 1.2 V, 250 mV s^{-1} scan rate, 30 cycles (last cycle shown, cleaned)). A Pt plate was used as a counter electrode and an Ag/AgCl as a reference electrode.

caused by adsorbed materials on the electrode surface [48, 57]. EIS measurements indicated that the impedances of the electrodes were consistently ∼200 kΩ at 1 kHz (211 ± 89 kΩ; mean ± SE, $n = 60$ electrodes). This value lies within the range of electrode impedances that have been indicated as desirable for neural recording [58]. The consistency of the batch fabrication method across a single wafer to produce the sheath probes is further demonstrated in analyzing the post-clean EIS magnitude and phase plots for the same electrode across four different probes from the same wafer (figure 11). Comparisons between figures 10 and 11 further support this result as electrode impedance and phase are similar on the same probe and across multiple probes. Results of electrochemical characterization demonstrated that the thin-film Pt electrodes of the sheath probe exhibited satisfactory properties required for neural recording.

3.3. Coating methods

Scanning electron microscopy (SEM) was used to confirm the presence of MG on the probe surface (data not shown). Benchtop testing using a spectrophotometer (Epoch; BioTek Instruments, Inc., Winooski, VT) also confirmed the success of the coating method. Absorbance measurements at 242 nm indicated the presence and measured the amount of DEX loaded onto each probe (0.15 μg) and ELISA was also used to confirm the presence of NGF on the probe. All three techniques confirmed the efficacy of the sonication-assisted dip coating method in coating the dual-probe arrays.

3.4. In vitro insertion tests

In vitro insertion tests of the sheath probe were performed using agarose gel (figure 12). Results indicated that the acrylic support shuttle with microwires provided the handling robustness required for attachment to and movement with the stereotaxic apparatus with no additional strain. Following removal of the introducer tool from the gel, the dual-probe array remained within the model (figure 12(d)). However, upon closer inspection of the cross sectional area of the gel block during the withdrawal process, the probe withdrew upward

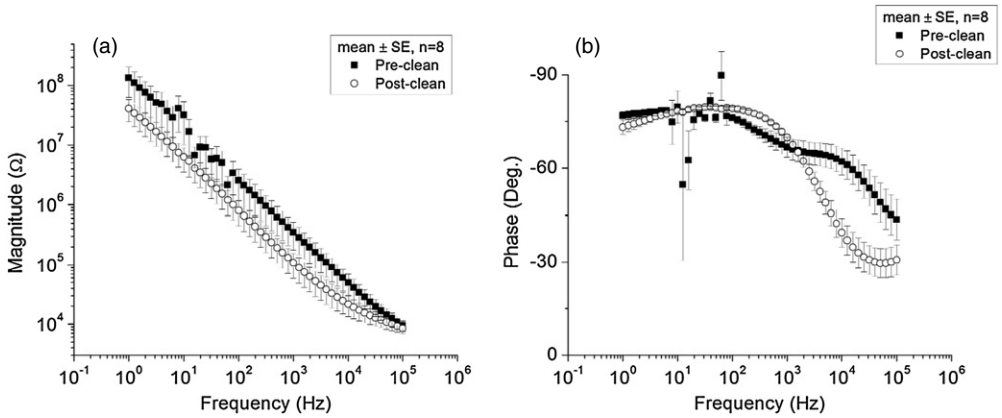

Figure 10. (a) Impedance magnitude plot of 8 electrodes of a single Parylene sheath probe pre-CV clean (black square) and post-CV clean (white square) (mean ± SE, $n = 8$ electrodes) measured in a beaker of 1 × PBS. Note that the magnitude decreased and discontinuities were removed, following the CV clean indicating the removal of adsorbed materials on the surface. (b) Corresponding impedance phase plot of sheath probe electrodes pre-CV clean (black square) and post-CV clean (white square) (mean ± SE, $n = 8$). The post-CV clean phase indicated the removal of multiple time constants also confirming removal of adsorbed materials.

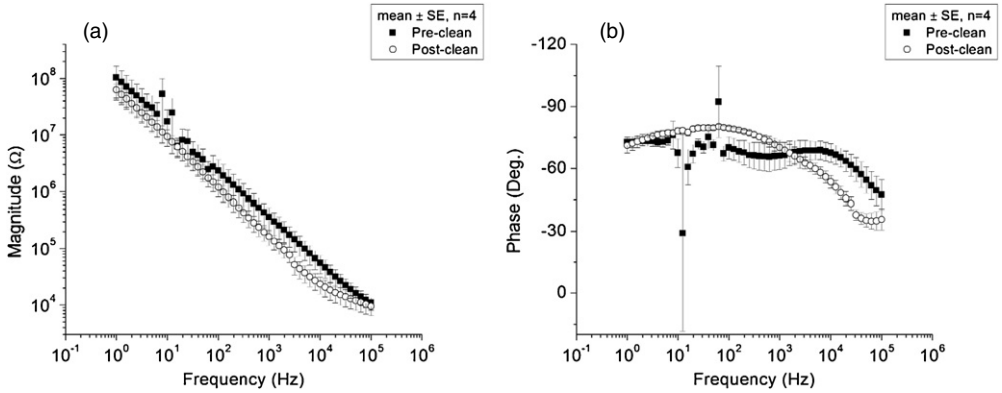

Figure 11. (a) Impedance magnitude plot of the same electrode on 4 different Parylene sheath probes from the same wafer pre-CV clean (black square) and post-CV clean (white square) (mean ± SE, n = 4 electrodes) measured in a beaker of 1 × PBS. (b) The corresponding impedance phase plot of the same electrodes across different sheath probes pre-CV clean (black square) and post-CV clean (white square) (mean ± SE, n = 4). Similar impedance magnitude and phase plots of the post-clean electrodes demonstrate consistency across sheath probes (in addition to figure 10).

86.34 ± 36.02 μm (mean ± SD, $n = 6$ trials) during retraction of the inserter tool (figure 13); this is likely attributed to surface tension at the PEG-inserter tool interface. To compensate for this, the surgery insertion depth for subsequent *in vivo* experiments was adjusted appropriately.

3.5. Cortical implantation and testing

The dual-probe arrays, assembled on the insertion tool, were manually inserted in the M1 motor cortex with a micromanipulator. The required insertion depth of 2 mm was achieved by stopping the insertion when the edge of the integrated Parylene cable (being considerably wider than the probe itself, as seen on figure 13) has touched the dural surface. To ensure proper insertion, placement, and depth utilizing the array-tool assembly, several acute insertions were carried out. Animals were then perfusion-fixed, the cortex dissected, and probe tracks evaluated in 100 μm-thick tissue sections (unstained or Nissl stained). The measured probe tracks were 2.0 ± 0.1 mm in depth (data not shown), reflecting slight variability in the attachment of the probes to the microwires.

In chronically-implanted animals, the flexPCB was bone-cemented to the skull to stabilize the exposed ZIF contact pads. In total, 13 animals were chronically implanted with 21 functional probes. In two animals (one with MG only-coated probes and another with MG + DEX-coated probes), most of the recording sites had 1 kHz impedance values below 30 kΩ, since the first *in vivo* impedance measurement at seven days, and were excluded from further analysis. The 1 kHz impedance measurements in the remaining 11 animals (19 probes) were evaluated over a 28-day period; with 147 recording sites, or 7.7 sites per probe, remaining electrically intact. Weekly evaluation of 1 kHz impedance measurements over the 28-day period demonstrated a gradual rise and some stabilization of the impedances (figure 14(a)); this is consistent with previously reported rise in the electrode impedance over time caused by electrode encapsulation *in vivo* [13]. Electrophysiological recordings were also made in weekly intervals and used to calculate the noise as well as the SNR

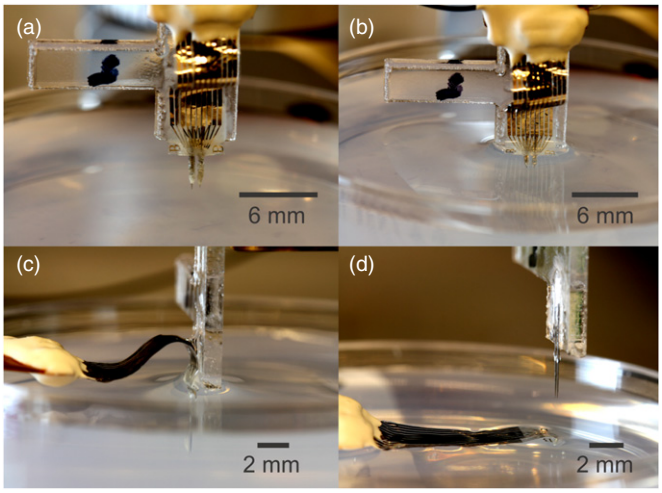

Figure 12. Image sequence of a representative *in vitro* agarose insertion test. (a) The array-tool assembly was attached to stereotaxic apparatus and positioned over the spot of interest. (b) The array-tool assembly was inserted into the agarose by hand, and 1 × PBS applied to begin the dissolution of PEG. (c) The dual-probe array was detached from the tool to allow for tool withdrawal; note that the Parylene cable was still attached to the tool. (d) After complete dissolution of PEG (5 min), the inserter tool was withdrawn from the agarose, and the dual-probe array remained implanted.

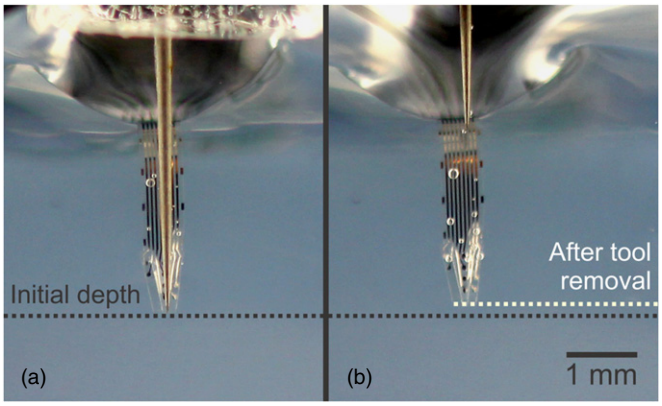

Figure 13. Image sequence of *in vitro* insertion test indicating that the probe withdrew ∼90 μm following the tool removal. (a) A photograph taken after insertion but prior to tool withdrawal where the probe tip depth is indicated by the black dotted line. (b) A photograph following tool withdrawal where the new probe tip depth is indicated by the white dotted line.

and the event rates of the detected multiunit neuronal activity (figures 14(b)–(d) and 15). At day 0, immediately after the probe implantation, the noise level was very low and there were practically no detectable spikes (figure 15(a)); while at day 14, the noise had increased several-fold and multiunit activity was readily picked up (figure 15(b)). The noise increased the most during the first 14–21 days (figure 14(c)), while the SNR and event rate continued to increase gradually over the 28-day period (figures 14(b) and (d)), suggesting an ongoing stabilization of the probe-tissue interface.

To evaluate the effects of varying drugs in the probe coating and varying probe tip shapes, data collected at 3–4 weeks post-implantation was used for the analysis (figures 16 and 17), as it represented a more stable tissue-electrode interface with a glial sheath around the probe. The comparison of coatings (figure 16) indicated no clear benefits of MG + NTC and MG + DEX coating for the SNR and noise parameters, yet a significant improvement in the event rate, as compared to the MG coating alone.

Comparison of the three probe tip designs indicated that the sharp tapered tip (type A) was more beneficial *in vivo* than the moderate-tapered tip (type B), which in turn was more beneficial than the blunt cylindrical tip (type C). As seen in figure 17, noise with the tapered designs A and B was higher than with the cylindrical probe, and the sharpest tip design A had significantly better SNRs than other designs.

Finally, the comparison of performances of the inner versus outer recording sites indicated that the outer sites achieved significantly higher SNR and noise values, with the impedance and event rate metrics showing the similar trend but their differences not being statistically significant (figure 18).

Immunohistochemical tissue analysis was performed for all 13 animals in the study. There was considerable variability in NeuN and GFAP staining both within and between the animals. Representative double-stained images for the three probe tip designs are shown (figure 19). Despite an observable trend toward higher neuronal density and lower GFAP density around the sharp tips, we found no statistically significant difference among the probe tip groups (figure 20), Plotting of the relative neuronal density versus the astrocytic density indicated a negative linear correlation with an $R^2 = 0.47$ (data not shown). Plotting of the electrophysiological versus the immunohistochemical parameters demonstrated that a better physiological performance correlated with a better preservation of neurons and reduced reactive astrocytic response (figure 21). The percentage of functionally active sites per probe and their average SNR values were both strongly correlated with the astrocytic density (figures 21(b) and (d)) and less strongly – with the neuronal density (figures 21(a) and (c)). There was no statistically significant linear correlation between the event rate and the neuronal or astrocytic density (data not shown).

4. Discussion

A Parylene neural probe with a 3D sheath structure to allow for the ingrowth of neural processes was fabricated, packaged, and validated in both *in vitro* and *in vivo* test settings for chronic implantation applications. Utilizing the thermoformable property of thin film Parylene, thermal molding of a 3D sheath structure was accomplished by inserting a microwire mold into a surface micromachined Parylene microchannel and performing a vacuum thermoforming process on the assembly. Eight Pt electrode sites were patterned on the inner and outer regions of the sheath to allow for multiple recording sites. The outer electrodes were moved to the perimeter of the probe to prevent electrode cracking due to the mechanical strain from the insertion of the microwire mold, experienced in the previous electrode layout on top of the sheath. The change in design also allowed for a simplification of the probe fabrication process, which improved electrode and probe yield. Reliability

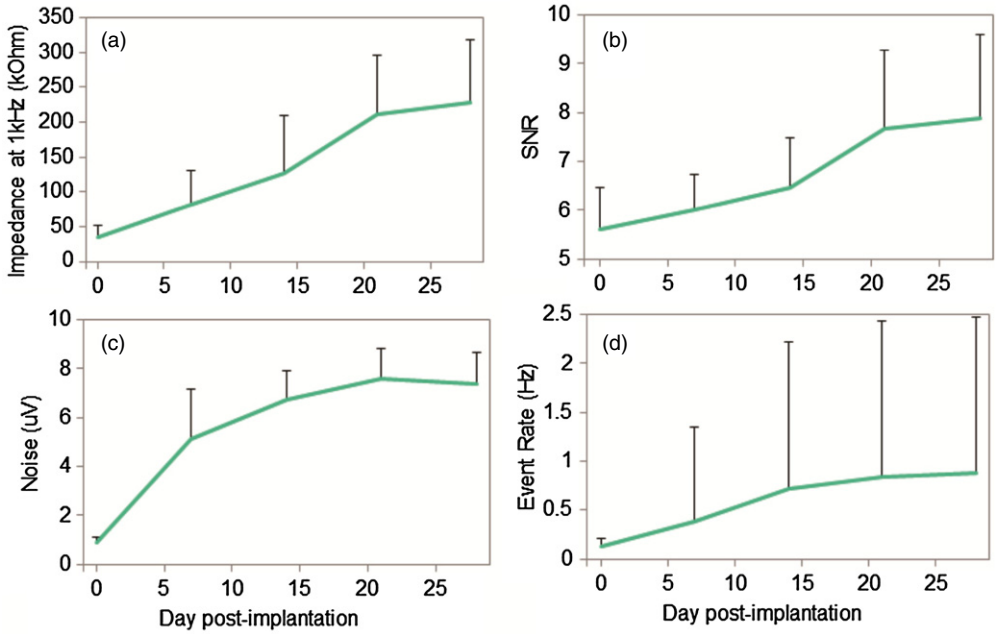

Figure 14. Changes in (a) 1 kHz impedance, (b) SNR, (c) noise, and (d) event rate over time after the probe implantation (mean ± SD, $n = 37$ recording sites in five probes). The selected five probes are from three animals (1 with probes A and 2 with probes B, 1 with MG + DEX coating and 2 with MG only coating), for which all weekly data were available.

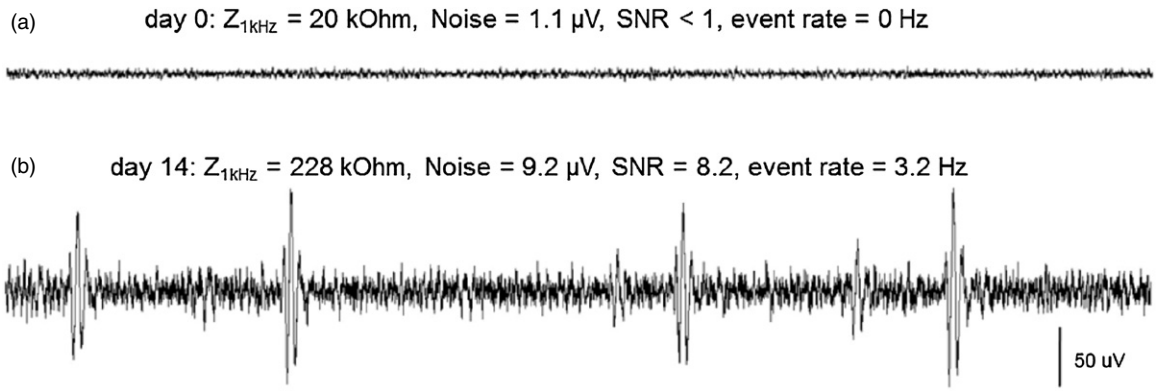

Figure 15. Representative electrophysiological traces at (a) day 0 and (b) day 14. Note a lack of resolvable neuronal activity at day 0 and emergence of well-resolved neuronal activity at day 14. The data are from the outer recording site on the probe B coated with MG only (animal MCX36). The key electrochemical and electrophysiological parameters for this recording site are noted above the traces.

of the dual-probe array interface was further improved by employing a custom designed flexPCB, whose ZIF contact pads allow for quick and repeatable connections from the probe to the measurement systems.

Electrochemical characterization of the electrodes of the sheath probe using CV and EIS aided in the cleaning of the electrode surface prior to implantation and confirmed electrode viability as well as the consistency of the batch fabrication method. Dual probe arrays were also uniformly coated with three different MG-based coating factors (containing either NTC, DEX, or no additives) using a sonically-assisted dip-coat technique. The compliant Parylene probe was successfully inserted into both *in vitro* and *in vivo* settings with the assistance of an introducer tool, allowing for proper and precise implantation of the dual-probe array, while limiting the damage to the surrounding tissue. Initial studies in rat demonstrated successful implantation of the dual-probe array and the bone cement head cap around the ZIF contact pad end of the flexPCB allowed the rat to be un-tethered during non-testing periods.

The performance of the Parylene sheath probe *in vivo* is difficult to directly compare with the NE, UEA, and MA largely due to the differences in the maturity of the technology as well as in surgical and electrophysiological measurement techniques (e.g., definition of SNR, noise, and event detection rates), but this study was completed with the aim of sheath probe development (coating and shape down-selection) and exploring its short term feasibility *in vivo*. In analyzing coating benefits on neurophysiological measurements over 28 days, some benefit on the event rate (but not on the SNR or noise) was observed by addition of the neurotrophic or immunosuppressant drugs to the MG coating. We speculate

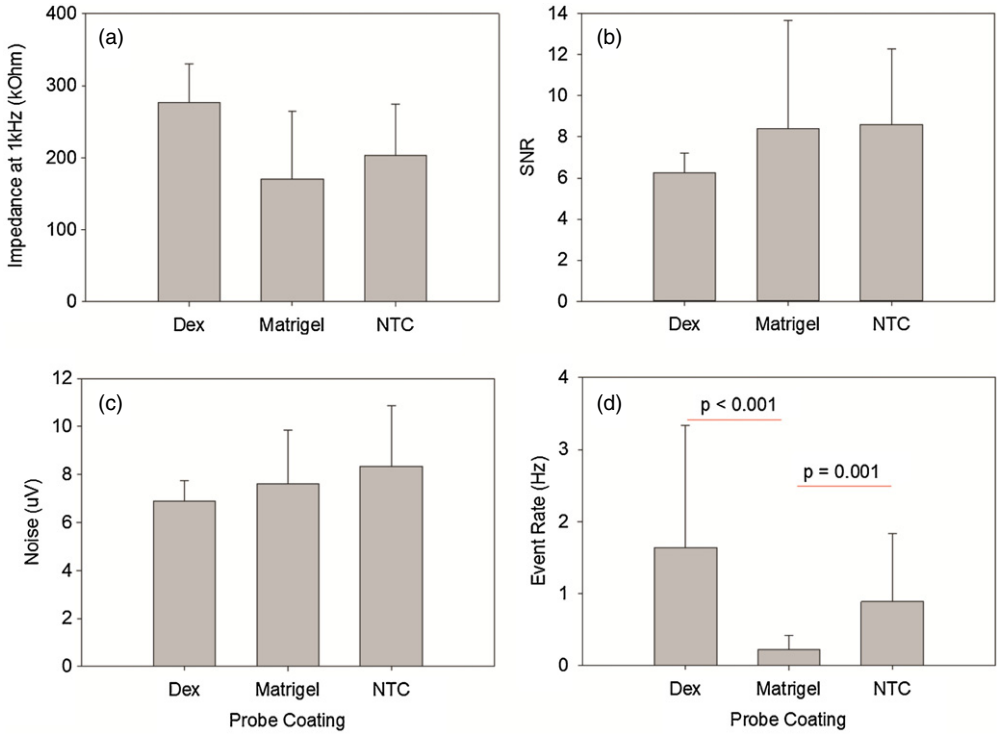

Figure 16. (a) 1 kHz impedance, (b) SNR, (c) noise, and (d) event rate measurement results obtained in comparing the different coatings at 28 days (mean ± SD, $n = 121$ recording sites in 9 animals, 16 probes). Only the design A and design B probes were included in this figure to avoid the confounding effect of the design C on the coating results. The design A probes ($n = 6$) all had MG only coating. The design B probes ($n = 10$) had the following coatings: MG + DEX ($n = 2$), MG only ($n = 4$), and MG + NTC ($n = 4$).

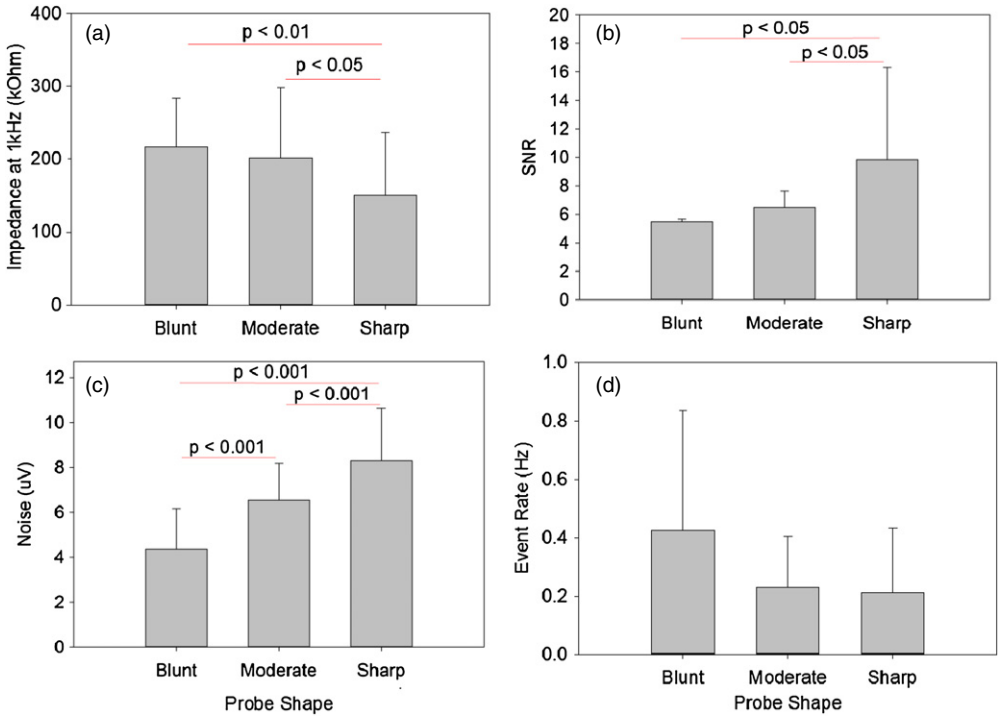

Figure 17. (a) 1 kHz impedance, (b) SNR, (c) noise, and (d) event rate measurement results obtained in comparing the different designs at 28 days (mean ± SD, $n = 103$ recording sites in seven animals, 13 probes). Designs were evaluated in probes with MG only coating (seven animals, 13 probes).

that the relatively small benefit of the factors was due to short implantation duration and/or rapid drug release from MG. Efforts in literature center around developing slower release coatings (∼1–2 weeks) of DEX [59] and NGF [60, 61] to provide a continual release of the factors during initial trauma and recovery and have demonstrated reduced

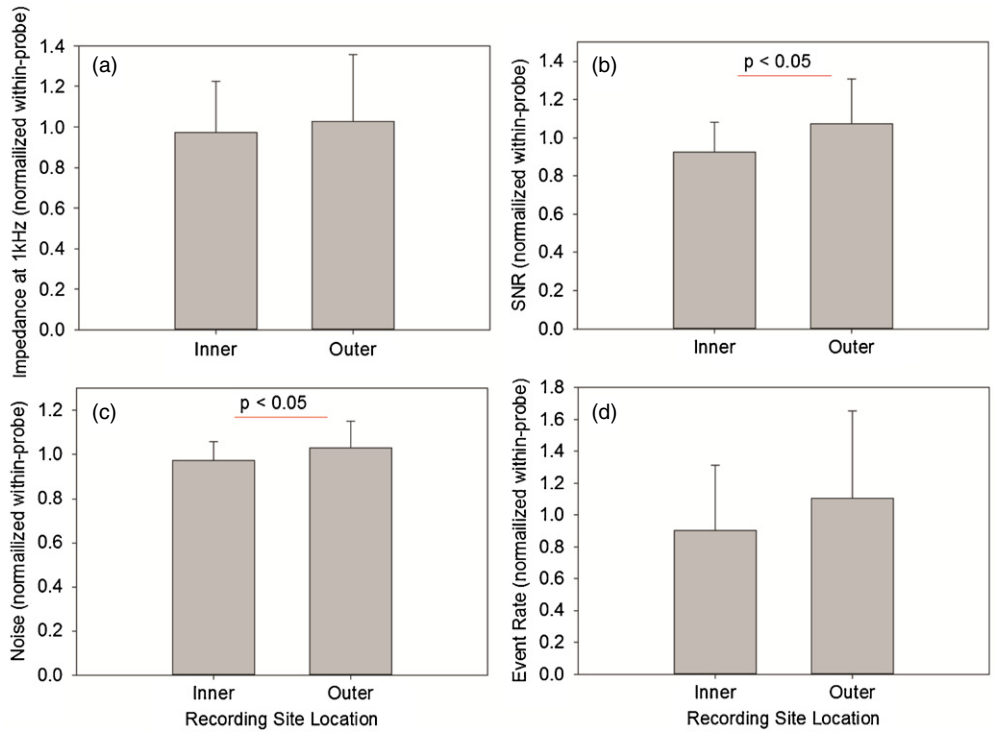

Figure 18. (a) 1 kHz impedance, (b) SNR, (c) noise, and (d) event rate measurement results obtained, comparing the inner electrodes from the outer electrodes at 28 days (mean $\pm$ SD, $n = 63$ recording sites in five animals, eight probes). The eight probes, selected for this figure, had 75% or more of their recording sites exhibiting the neuronal activity. Within-probe normalization of the parameters was performed in order to remove the confounding influences of the tip geometry and probe placement in the cortex. All selected probes had the MG only coating: four of them had the design A and the other four had the design B.

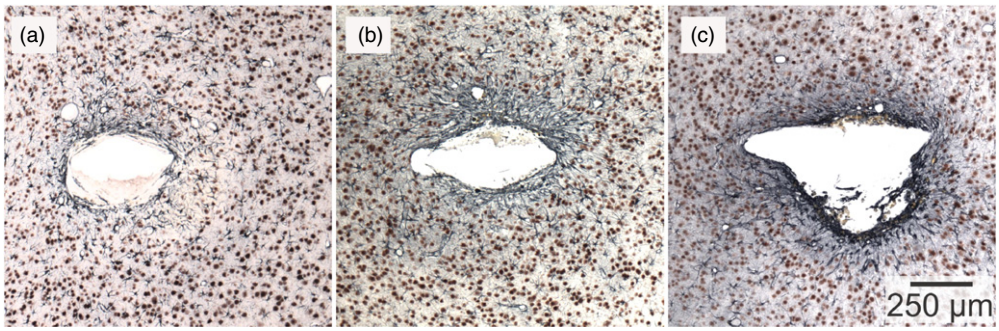

Figure 19. Sample microphotographs of the cerebral cortex double-stained with antibodies for NeuN (brown) and GFAP (dark-blue) through the following probe tips: (a) sharp, (b) moderate, and (c) blunt. The 10 μm sections were cut perpendicular to the probe track (the probe was removed during brain dissection).

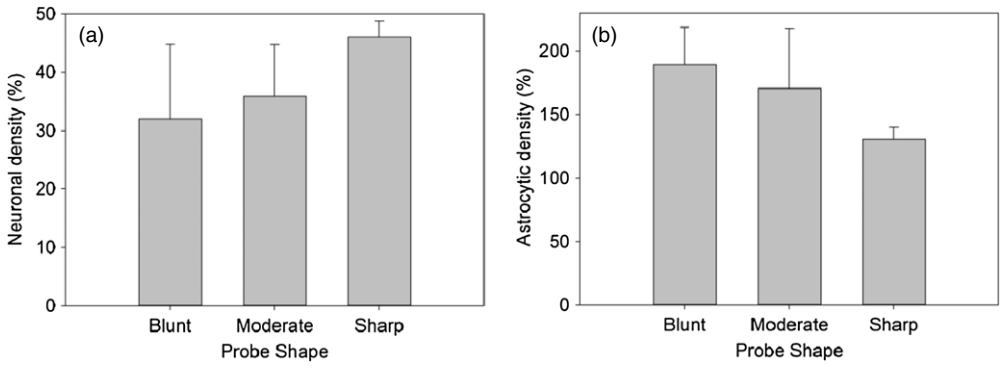

Figure 20. Quantification of (a) neuronal and (b) astrocytic density for different probe tip shapes (blunt, moderate, and sharp) at 28 days ($n = 13$ animals). Detailed description of the steps to calculate the neuronal and astrocytic density is provided in the *Methods* section.

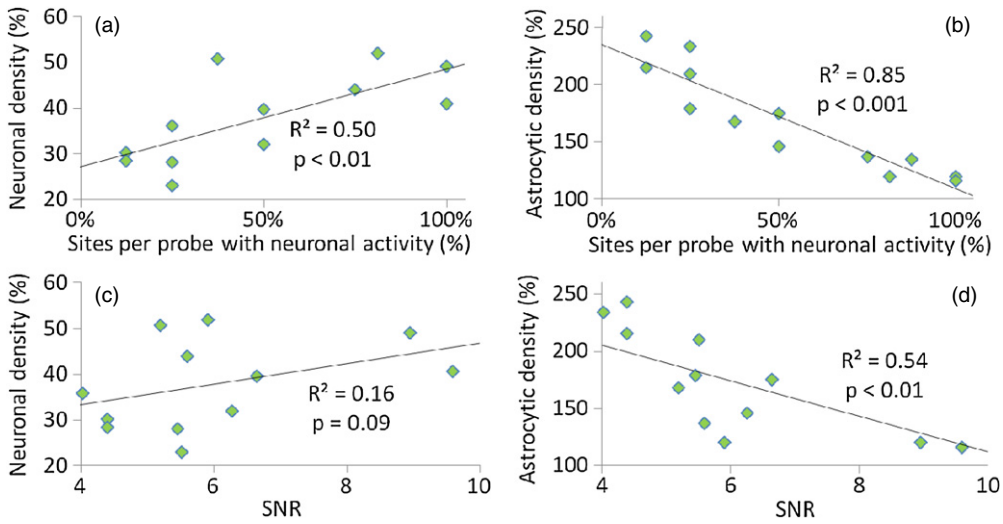

Figure 21. Plots of the electrophysiological against immunohistochemical parameters at 28 days ($n = 13$ animals). The electrophysiological parameters are: (a, b) percentage of functionally-active recording sites and (c, d) SNR. The immunohistochemical parameters are: (a, c) neuronal density and (b, d) astrocytic density near the probe track. R^2 indicates the square of Pearson's correlation coefficient. Detailed description of the steps to calculate the neuronal and astrocytic density is provided in the *Methods* section.

immune expression and enhanced neuronal growth with these methods. A subsequent study with a longer implantation time and prolonged drug release (spanning over weeks rather than hours) would be necessary to demonstrate the full extent of the ingrowth of neural processes, as suggested in prior studies [31]. The sharper tapered design achieved better performance *in vivo* than the blunt and moderate-taper designs, which may be attributed to additional damage of the surrounding tissue during/upon implantation caused by a blunt, larger tip compared to the sharper tapers. A trend toward higher astrocytic activation and reduced neuronal density was observed, but did not reach significance (possibly due to small sample numbers in blunt and sharp groups). Our results are further supported by a microscopically-monitored cortical insertion study, demonstrating that sharp tips do not produce more micro-vessel severance (compared to blunt tips); in contrast, blunt tips produce more tissue strain, resulting in dragging and subsequent rupture of microvascular networks [62]. The outer recording sites demonstrated better physiological performance, presumably due to their closer location to the neural tissue. Immunohistochemical evaluation indicated that the better-performing probes were surrounded with fewer reactive astrocytes and more viable neurons. These findings further support the importance of the neurotrophic and immunosuppressant drugs for maintaining and even improving the health of neural tissue around the probes and demonstrate the feasibility of the 3D Parylene sheath probes for chronic applications.

Though the results were inconclusive in the impact of the sheath design to encourage neural ingrowth, this study was vital in evaluating the design, fabrication, coating, and insertion strategies for development of a cortical interface using chronically implanted Parylene sheath probes. The Parylene substrate aims to improve tissue integration and reduces damage during cortical micromotion, but the flexible material makes handling and insertion difficult, and requires the development of packaging, handling, and insertion strategies to allow for robust implementation. For the sheath design, results indicated that 28 days is not sufficient for neural ingrowth into the sheath, and revealed that coating factors are beneficial but require a much slower release profile. Currently, work is underway to design and fabricate a sheath probe array of the sharp taper design with four or more probes to increase cortical coverage and remain implanted for a long-term study (>3 months). Both the fabrication process and insertion methods currently used for the double probes would be adapted for use with these arrays. Coating efficacy studies are ongoing to compare the effects of differing concentrations and combinations of coatings as well as extended release formulation to further improve long term probe reliability. Overall, the presented 28-day implantation results show the promise of 3D Parylene sheath neural probes for chronic neural recordings and as a viable alternative to microwire and silicon-based counterparts.

Acknowledgments

This work was sponsored by the Defense Advanced Research Projects Agency (DARPA) MTO under the auspices of Dr Jack Judy through the Space and Naval Warfare Systems Center, Pacific grant/contract no. N66001-11-1-4207. The authors would also like to thank the following individuals at the Huntington Medical Research Institutes: Dr Douglas McCreery for advice on probe development and introducer tool design, Ms Kate Nelson and Dr Saiyun Hou for performing the chronic animal implantations and transcardial perfusions, Ms Nijole Kuleviciute for collection of *in vivo* impedance spectroscopy data and for image analysis, Dr Martin Han for providing access to the electrophysiological recording system, Mr Jesus Chavez and Ms Annalee Stone for performing the tissue cutting and immunohistochemical staining. We also thank Dr Donghai Zhu of the Keck Photonics Laboratory for help with fabrication, and members of the Biomedical Microsystems Laboratory of USC for their assistance.

References

[1] Lebedev M A and Nicolelis M A L 2006 Brain–machine interfaces: past, present and future *Trends Neurosci.* **29** 536–46

[2] Nicolelis M A L 2003 Brain–machine interfaces to restore motor function and probe neural circuits *Nature Rev. Neurosci.* **4** 417–22

[3] Kipke D R, Vetter R J, Williams J C and Hetke J F 2003 Silicon-substrate intracortical microelectrode arrays for long-term recording of neuronal spike activity in cerebral cortex *IEEE Trans. Neural Syst. Rehabil.* **11** 151–5

[4] Rousche P J and Normann R A 1998 Chronic recording capability of the Utah intracortical electrode array in cat sensory cortex *J. Neurosci. Methods* **82** 1–15

[5] Vetter R J, Williams J C, Hetke J F, Nunamaker E A and Kipke D R 2004 Chronic neural recording using silicon-substrate microelectrode arrays implanted in cerebral cortex *IEEE Trans. Biomed. Eng.* **51** 896–904

[6] Campbell P K, Jones K E, Huber R J, Horch K W and Normann R A 1991 A silicon-based, three-dimensional neural interface: manufacturing processes for an intracortical electrode array *IEEE Trans. Biomed. Eng.* **38** 758–68

[7] Najafi K and Wise K D 1986 An implantable multielectrode array with on-chip signal processing *IEEE J. Solid-State Circuits* **21** 1035–44

[8] Maynard E M, Hatsopoulos N G, Ojakangas C L, Acuna B D, Sanes J N, Normann R A and Donoghue J P 1999 Neuronal interactions improve cortical population coding of movement direction *J. Neurosci.* **19** 8083–93

[9] Suner S, Fellows M R, Vargas-Irwin C, Nakata G K and Donoghue J P 2005 Reliability of signals from a chronically implanted, silicon-based electrode array in non-human primate primary motor cortex *IEEE Trans. Neural Syst. Rehabil. Eng.* **13** 524–41

[10] Hochberg L R, Serruya M D, Friehs G M, Mukand J A, Saleh M, Caplan A H, Branner A, Chen D, Penn R D and Donoghue J P 2006 Neuronal ensemble control of prosthetic devices by a human with tetraplegia *Nature* **442** 164–71

[11] Sodagar A M, Perlin G E, Ying Y, Najafi K and Wise K D 2009 An implantable 64-channel wireless microsystem for single-unit neural recording *IEEE J. Solid-State Circuits* **44** 2591–604

[12] Perlin G E and Wise K D 2008 A compact architecture for three-dimensional neural microelectrode arrays *30th Annu. Int. Conf. of the IEEE Engineering in Medicine and Biology Society* pp 5806–9

[13] Abhishek P and Justin C S 2012 Quantifying long-term microelectrode array functionality using chronic *in vivo* impedance testing *J. Neural Eng.* **9** 026028

[14] Ward M P, Rajdev P, Ellison C and Irazoqui P P 2009 Toward a comparison of microelectrodes for acute and chronic recordings *Brain Res* **1282** 183–200

[15] McConnell G C, Rees H D, Levey A I, Gutekunst C A, Gross R E and Bellamkonda R V 2009 Implanted neural electrodes cause chronic, local inflammation that is correlated with local neurodegeneration *J Neural Eng.* **6** 056003

[16] Szarowski D H, Andersen M D, Retterer S, Spence A J, Isaacson M, Craighead H G, Turner J N and Shain W 2003 Brain responses to micro-machined silicon devices *Brain Res* **983** 23–35

[17] Gilletti A and Muthuswamy J 2006 Brain micromotion around implants in the rodent somatosensory cortex *J. Neural Eng.* **3** 189–95

[18] Turner J N, Shain W, Szarowski D H, Andersen M, Martins S, Isaacson M and Craighead H 1999 Cerebral astrocyte response to micromachined silicon implants *Exp. Neurol.* **156** 33–49

[19] Kim Y-T, Hitchcock R W, Bridge M J and Tresco P A 2004 Chronic response of adult rat brain tissue to implants anchored to the skull *Biomaterials* **25** 2229–37

[20] Rousche P J, Pellinen D S, Pivin D P Jr, Williams J C, Vetter R J and Kirke D R 2001 Flexible polyimide-based intracortical electrode arrays with bioactive capability *IEEE Trans. Biomed. Eng.* **48** 361–71

[21] Takeuchi S, Ziegler D, Yoshida Y, Mabuchi K and Suzuki T 2005 Parylene flexible neural probes integrated with microfluidic channels *Lab Chip* **5** 519–23

[22] Lee S E, Jun S B, Lee H J, Kim J, Lee S W, Im C, Shin H C, Chang J W and Kim S J 2012 A flexible depth probe using liquid crystal polymer *IEEE Trans. Biomed. Eng.* **59** 2085–94

[23] Andrei A, Tutunjyan N, Verbinnen G, VanPut S, Krylychkina O, Eberle W and Musa S 2012 Fabrication and successful *in-vivo* implantation of a flexible neural implant with a hybrid polyimide-silicon design *Annu. Int. Conf. of the IEEE Engineering in Medicine and Biology Society* pp 3890–3

[24] Fomani A and Mansour R R 2011 Fabrication and characterization of the flexible neural microprobes with improved structural design *Sensors Actuators* A **168** 233–41

[25] Egert D, Peterson R L and Najafi K 2011 Parylene microprobes with engineered stiffness and shape for improved insertion *16th Int. Conf. Solid-State Sensors, Actuators and Microsystems* pp 198–201

[26] Seymour J P and Kipke D R 2006 Fabrication of polymer neural probes with sub-cellular features for reduced tissue encapsulation *28th Annu. Int. Conf. of the IEEE Engineering in Medicine and Biology Society* pp 4606–9

[27] Fan W, Maesoon I and Euisik Y 2011 A flexible fish-bone-shaped neural probe strengthened by biodegradable silk coating for enhanced biocompatibility *16th Int. Conf. Solid-State Sensors, Actuators and Microsystems* pp 966–9

[28] Kennedy P, Andreasen D, Ehirim P, King B, Kirby T, Mao H and Moore M 2004 Using human extra-cortical local field potentials to control a switch *J. Neural Eng.* **1** 72

[29] Kennedy P R 1989 The cone electrode: a long-term electrode that records from neurites grown onto its recording surface *J. Neurosci. Methods* **29** 181–93

[30] Kennedy P R and Bakay R A 1998 Restoration of neural output from a paralyzed patient by a direct brain connection *Neuroreport* **9** 1707–11

[31] Kennedy P R, Mirra S S and Bakay R A E 1992 The cone electrode: ultrastructural studies following long-term recording in rat and monkey cortex *Neurosci. Lett.* **142** 89–94

[32] Kennedy P R, Bakay R A and Sharpe S M 1992 Behavioral correlates of action potentials recorded chronically inside the cone electrode *Neuroreport* **3** 605–8

[33] Bartels J, Andreasen D, Ehirim P, Mao H, Seibert S, Wright E J and Kennedy P 2008 Neurotrophic electrode: method of assembly and implantation into human motor speech cortex *J. Neurosci. Methods* **174** 168–76

[34] Eaton K P and Henriquez C S 2005 Confounded spikes generated by synchrony within neural tissue models *Neurocomputing* **65** 851–7

[35] Kuo J T W, Kim B J, Hara S A, Lee C, Gutierrez C A, Hoang T and Meng E 2012 Fabrication of 3D Parylene sheath probes for reliable neuroprosthetic recordings *Hilton Head 2012: Solid State Sensors, Actuators and Microsystems Workshop (Hilton Head Island, SC)* pp 30–3

[36] Huang R and Tai Y-C 2010 Flexible Parylene-based 3D coiled cable *5th IEEE Int. Conf. on Nano/Micro Engineered and Molecular Systems* pp 317–20

[37] Meng E, Li P Y and Tai Y C 2008 Plasma removal of Parylene C *J. Micromech. Microeng.* **18** 045004
[38] Shih C, Harder T A and Tai Y C 2004 Yield strength of thin-film Parylene-C *Microsyst. Technol.* **10** 407–11
[39] Meng E 2010 *Biomedical Microsystems* (Boca Raton, FL: CRC Press)
[40] Vasenkov A V 2011 Atomistic modeling of Parylene–metal interactions for surface micro-structuring *J. Mol. Modeling* **17** 3219–28
[41] Lee J H, Hwang K S, Yoon K H, Kim T S and Ahn S 2004 Microstructure and adhesion of Au deposited on Parylene-c substrate with surface modification for potential immunoassay application *IEEE Trans. Plasma Sci.* **32** 505–9
[42] Kahouli A, Sylvestre A, Jomni F, Yangui B and Legrand J 2012 Ac-conductivity and dielectric relaxations above glass transition temperature for Parylene-C thin films *Appl. Phys.* A **106** 909–13
[43] Noh H-S, Huang Y and Hesketh P J 2004 Parylene micromolding, a rapid and low-cost fabrication method for Parylene microchannel *Sensors Actuators* B **102** 78–85
[44] Hsu J-M, Rieth L, Kammer S, Orthner M and Solzbacher F 2008 Effect of thermal and deposition processes on surface morphology, crystallinity, and adhesion of Parylene-C *Sensors Mater.* **20** 71–86
[45] Grattan D W and Bilz M 1991 The thermal aging of Parylene and the effect of antioxidant *Stud. Conserv.* **36** 44–52
[46] Huang R and Tai Y C 2009 Parylene to silicon adhesion enhancement *Int. Conf. Solid-State Sensors, Actuators and Microsystems* pp 1027–30
[47] Gutierrez C A, Lee C, Kim B and Meng E 2011 Epoxy-less packaging methods for electrical contact to parylene-based flat flexible cables *16th Int. Conf. Solid-State Sensors, Actuators and Microsystems* pp 2299–302
[48] Hara S, Kim B J, Kuo J T W, Lee C, Gutierrez C A, Hoang T and Meng E 2012 Pre-implantation electrochemical characterization of a Parylene C sheath microelectrode array probe *Int. Conf. of the IEEE Engineering in Medicine and Biology Society (San Diego, CA)* pp 512–9
[49] Passaniti A, Taylor R M, Pili R, Guo Y, Long P V, Haney J A, Pauly R R, Grant D S and Martin G R 1992 Methods in laboratory investigation—a simple, quantitative method for assessing angiogenesis and antiangiogenic agents using reconstituted basement-membrane, heparin, and fibroblast growth-factor *Lab. Invest.* **67** 519–28
[50] Kozai T D Y and Kipke D R 2009 Insertion shuttle with carboxyl terminated self-assembled monolayer coatings for implanting flexible polymer neural probes in the brain *J. Neurosci. Methods* **184** 199–205
[51] Chen Z J, Gillies G T, Broaddus W C, Prabhu S S, Fillmore H, Mitchell R M, Corwin F D and Fatouros P P 2004 A realistic brain tissue phantom for intraparenchymal infusion studies *J. Neurosurg.* **101** 314–22
[52] Pervin F and Chen W W 2010 Mechanically similar Gel simulants for brain tissues *Ann. Conf. SEM (Indianapolis, IN)* pp 9–13
[53] Sigma Aldrich Inc. Nerve growth factor-2.5S (N6009) Datasheet www.sigmaaldrich.com/
[54] Gibson S, Judy J W and Markovic D 2010 Technology-aware algorithm design for neural spike detection, feature extraction, and dimensionality reduction *IEEE Trans. Neural Syst. Rehabil. Eng.* **18** pp 469–78
[55] Li W, Rodger D C, Menon P R and Tai Y C 2008 Corrosion behavior of parylene–metal–parylene thin films in saline *ECS Trans.* **11** 1–6
[56] Kim B J, Chen B, Gupta M and Meng E 2013 Three dimensional transformation of Parylene thin film structures via thermoforming *26th IEEE Int. Conf. on Micro Electro Mechanical Systems (Taipei, Taiwan)* pp 339–42
[57] Sawyer D T 1974 *Experimental Electrochemistry for Chemists* (New York: Wiley) pp 60–100
[58] Cogan S F 2008 Neural stimulation and recording electrodes *Annu. Rev. Biomed. Eng.* **10** 275–309
[59] Zhong Y and Bellamkonda R V 2007 Dexamethasone-coated neural probes elicit attenuated inflammatory response and neuronal loss compared to uncoated neural probes *Brain Res* **1148** 15–27
[60] Kato Y, Saito I, Hoshino T, Suzuki T and Mabuchi K 2006 Preliminary study of multichannel flexible neural probes coated with hybrid biodegradable polymer *28th Annu. Int. Conf. of the IEEE Engineering in Medicine and Biology Society* pp 660–3
[61] Winter J O, Cogan S F and Rizzo J F 2007 Neurotrophin-eluting hydrogel coatings for neural stimulating electrodes *J. Biomed. Mater. Res.* B **81** 551–63
[62] Bjornsson C S, Oh S J, Al-Kofahi Y A, Lim Y J, Smith K L, Turner J N, De S, Roysam B, Shain W and Kim S J 2006 Effects of insertion conditions on tissue strain and vascular damage during neuroprosthetic device insertion *J. Neural Eng.* **3** 196